AGU PUBLICATIONS

Paleoceanography

RESEARCH ARTICLE

10.1002/2015PA002868

Similar millennial climate variability on the Iberian margin during two early Pleistocene glacials and MIS 3

B. Birner[1], D. A. Hodell[1], P. C. Tzedakis[2], and L. C. Skinner[1]

[1]Godwin Laboratory for Palaeoclimate Research, Department of Earth Sciences, University of Cambridge, Cambridge, UK, [2]UCL Department of Geography, University College London, London, UK

Key Points:
- Millennial variability was a pervasive feature of early Pleistocene climate
- Millennial variability in MIS 38 and 40 resembled Dansgaard-Oeschger cycles of MIS 3
- The bipolar see-saw was active during most major stadials in the early Pleistocene

Supporting Information:
- Texts S1–S5, Figures S1–S7, and Tables S1 and S2

Correspondence to:
B. Birner,
bbirner@ucsd.edu

Citation:
Birner, B., D. A. Hodell, P. C. Tzedakis, and L. C. Skinner (2016), Similar millennial climate variability on the Iberian margin during two early Pleistocene glacials and MIS 3, *Paleoceanography*, *31*, 203–217, doi:10.1002/2015PA002868.

Received 5 AUG 2015
Accepted 15 DEC 2015
Accepted article online 17 DEC 2015
Published online 28 JAN 2016

Abstract Although millennial-scale climate variability (<10 ka) has been well studied during the last glacial cycles, little is known about this important aspect of climate in the early Pleistocene, prior to the Middle Pleistocene Transition. Here we present an early Pleistocene climate record at centennial resolution for two representative glacials (marine isotope stages (MIS) 37–41 from approximately 1235 to 1320 ka) during the "41 ka world" at Integrated Ocean Drilling Program Site U1385 (the "Shackleton Site") on the southwest Iberian margin. Millennial-scale climate variability was suppressed during interglacial periods (MIS 37, MIS 39, and MIS 41) and activated during glacial inceptions when benthic $\delta^{18}O$ exceeded 3.2‰. Millennial variability during glacials MIS 38 and MIS 40 closely resembled Dansgaard-Oeschger events from the last glacial (MIS 3) in amplitude, shape, and pacing. The phasing of oxygen and carbon isotope variability is consistent with an active oceanic thermal bipolar see-saw between the Northern and Southern Hemispheres during most of the prominent stadials. Surface cooling was associated with systematic decreases in benthic carbon isotopes, indicating concomitant changes in the meridional overturning circulation. A comparison to other North Atlantic records of ice rafting during the early Pleistocene suggests that freshwater forcing, as proposed for the late Pleistocene, was involved in triggering or amplifying perturbations of the North Atlantic circulation that elicited a bipolar see-saw response. Our findings support similarities in the operation of the climate system occurring on millennial time scales before and after the Middle Pleistocene Transition despite the increases in global ice volume and duration of the glacial cycles.

1. Introduction

Earth's climate system during the Pleistocene alternated between glacial and interglacial conditions upon which millennial-scale variability was frequently superimposed. The nature of suborbital variability has been well documented for the last 800,000 years from Greenland and Antarctic ice cores [*Dansgaard et al.*, 1993; *Jouzel et al.*, 2007; *European Project for Ice Coring in Antarctica Community Members*, 2006; *Johnsen et al.*, 1992; *Oeschger et al.*, 1984] as well as marine sediment records [*Shackleton et al.*, 2000; *Bond et al.*, 1993; *Bond and Lotti*, 1995; *McManus et al.*, 1999; *Margari et al.*, 2010]; however, little is known about millennial-scale variability under the different climatic boundary conditions of the early Pleistocene (herein informally referring to the period 1–2.58 million years ago) when ice volume was smaller and the duration of glacial cycles shorter than during the late Pleistocene (herein informally defined as the last 1 million years). In the early Pleistocene, glacial-interglacial cycles occurred every 41,000 years (the "41 ka world"), corresponding to the period of the Earth's obliquity cycle, whereas in the late Pleistocene, the glacial-interglacial cycles were quasi-periodic, repeating approximately every 100,000 years (the "100 ka world"). In contrast to the sawtooth-shaped, asymmetric glacial cycles of the 100 ka world, the 41 ka cycles were more symmetric, suggesting that climate variables, ice volume in particular, responded almost linearly to orbital insolation forcing [*Raymo and Nisancioglu*, 2003; *Imbrie et al.*, 1992, 1993; *Maslin and Brierley*, 2015]. However, recent work has questioned the symmetry and simple linearity of glacial cycles in the early Pleistocene climate system [*Ashkenazy and Tziperman*, 2004; *Lourens et al.*, 2010]. The difference in climate response to the same orbital forcing before and after the Middle Pleistocene Transition (MPT, ~650–1100 ka) has commonly been attributed to the smaller ice volumes (~50 m sea level equivalent) in the 41 ka world [*Elderfield et al.*, 2012; *Rohling et al.*, 2014; *Clark et al.*, 2006], but the exact cause remains unknown.

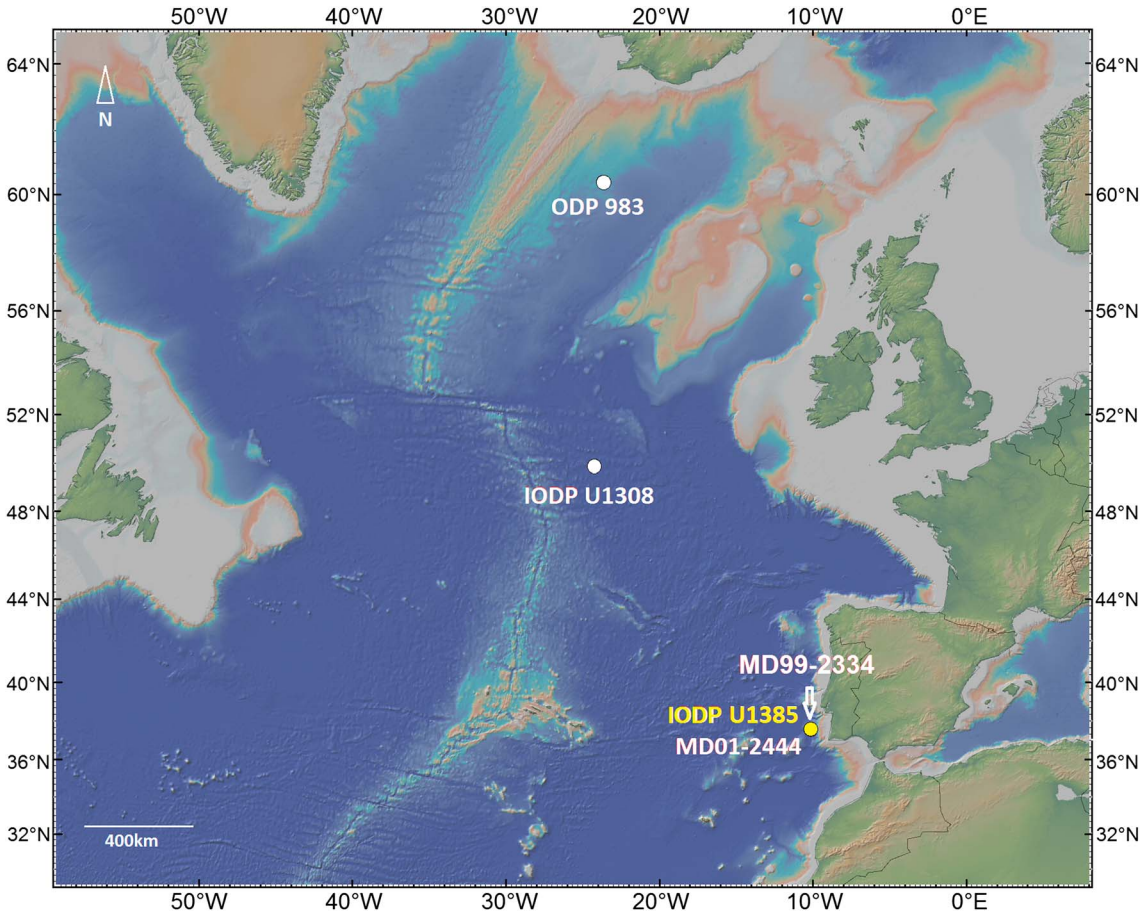

Figure 1. Locations of Integrated Ocean Drilling Program (IODP) sites and piston cores referred to in this study. Site U1385 (37°34.285′N, 10°7.562′W, water depth = 2578 m) was drilled on the SW Iberian margin at the same location as core MD01-2444. Piston core MD99-2334 (37°48′N, 10°10′W, water depth = 3246 m) was recovered 26 km to the north. IODP Site U1308 (49°53′N, 24°14′W, water depth = 3871 m) used by *Hodell et al.* [2008] is a reoccupation of Deep Sea Drilling Project Site 609, and Ocean Drilling Program Ocean Drilling Program ODP Site 983 (60°24′N, 23°38′W, water depth = 1983 m) is located on the Garder drift near Iceland [*Raymo et al.*, 1998]. Basemap data are from *Ryan et al.* [2009].

Substantial climate variability occurred also on suborbital time scales throughout the Pleistocene and may have affected the pattern of glacial-interglacial cycles [*McManus et al.*, 1999; *Raymo et al.*, 1998; *Barker et al.*, 2011; *Jouzel et al.*, 2007; *Denton et al.*, 2010]. Our understanding of millennial events is, however, strongly biased by the last several glaciations because evidence of millennial climate variability in the early Pleistocene is scarce. *Raymo et al.* [1998] first reported considerable millennial variability in ice-rafted debris (IRD) counts and benthic $\delta^{13}C$ values for marine isotope stages (MIS) 40 and 44 (approximately between 1.3 and 1.4 million years ago). Coupled changes of both proxies also suggested a potential link between ice rafting and perturbations of the Atlantic meridional overturning circulation (AMOC), but the resolution of the record was too low to be conclusive. *Mc Intyre et al.* [2001] observed IRD events during 1.75–1.83 Ma that recurred every ~2–5 ka comparable to the pacing of millennial variability in the late Pleistocene. Heinrich events, however, have only been identified in late Pleistocene glaciations after 640 ka and were presumably absent in the early Pleistocene [*Hodell et al.*, 2008]. Some studies have indicated that millennial-scale variability increased across the MPT as ice volume expanded [*Weirauch et al.*, 2008], whereas others have observed persistently strong millennial variability in the early Pleistocene [*Raymo et al.*, 1998; *Tzedakis et al.*, 2015; *Grützner and Higgins*, 2010; *Hodell et al.*, 2008].

Because the climate response to the same orbital forcing changed substantially across the MPT (e.g., increasing ice volume and duration of glacial cycles), the 41 ka world provides a natural (historical) experiment to study the nature of millennial variability under different climatic boundary conditions than during the 100 ka world. To improve our understanding of millennial events and their significance for the theory of Pleistocene ice ages, we studied millennial-scale climate variability at the Integrated Ocean Drilling Program (IODP) Site

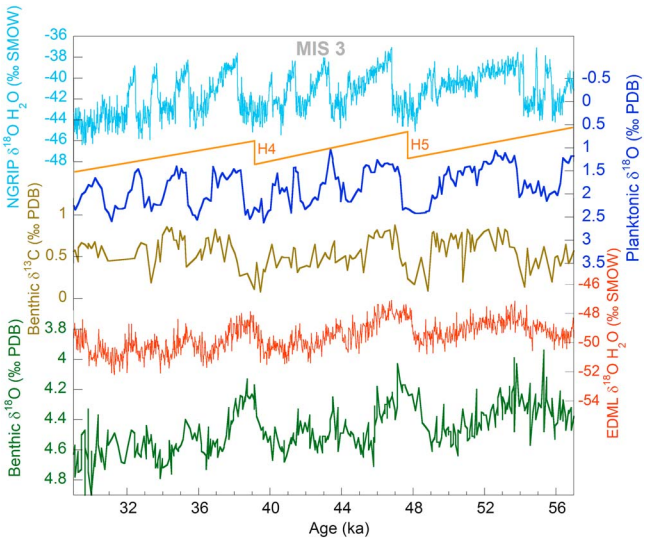

Figure 2. Comparison of planktonic δ^{18}O (*G. bulloides*), benthic δ^{13}C (*C. Wuellerstorfi*), and benthic δ^{18}O (mixed species) from core MD01-2444 [*Skinner et al.*, 2007; *Vautravers and Shackleton*, 2006] to the NGRIP [*North Greenland Ice Core Project Members*, 2004] and the EPICA Dronning Maud Land [*European Project for Ice Coring in Antarctica Community Members*, 2006] δ^{18}O records on the AICC2012 synchronized time scale [*Bazin et al.*, 2013]. Orange lines indicate the grouping of Dansgaard-Oeschger (D-O) events into Bond cycles [*Bond et al.*, 1997] that are bounded by Heinrich events H3 to H6.

U1385 on the Iberian margin off the Portuguese coast (~37°N, 10°W, Figure 1). Two glacial-interglacial cycles (MIS 37–39 and MIS 39–41) were selected during the early Pleistocene because they represent one strong and one weak glacial cycle, respectively. The interval is well suited for an assessment of early Pleistocene climate as the 41 ka periodicity characteristic of many early Pleistocene ice age cycles was well established during this interval [*Lisiecki and Raymo*, 2005] and the MPT had not yet begun. The new observations are compared to data of the last glacial cycle from piston cores taken closeby to Site U1385.

1.1. The Iberian Margin

The Iberian margin is a prime location to study millennial-scale climate variability, because during the last glacial cycle the isotope records of planktonic and benthic foraminifera from this region simultaneously recorded rapid climate change expressed in Greenland and Antarctic ice cores, respectively [*Shackleton et al.*, 2000, 2004] (Figure 2). Local sea surface temperature and hence δ^{18}O of planktonic foraminifera are linked to temperature in Greenland by migrations of the Polar Front that reached as far south as 39°N during Heinrich events [*Voelker and de Abreu*, 2011]. *Shackleton et al.* [2000] showed that each Dansgaard-Oeschger event (D-O event) coincided with a δ^{18}O change of 0.8‰ to 1.2‰ in *Globigerina bulloides* at the Iberian margin. The D-O cooling occurred more gradually than the abrupt terminal warming giving rise to a characteristic sawtooth pattern [*Shackleton et al.*, 2000] that repeated approximately every 1500 years or multiples thereof [*Schulz*, 2002].

The δ^{18}O changes of benthic foraminifera in the same sediment core closely resemble the Antarctic temperature record [*Shackleton et al.*, 2000, 2004; *Skinner et al.*, 2003; *Margari et al.*, 2010, 2014; *Martrat et al.*, 2007]. The millennial-scale benthic δ^{18}O signal in Iberian margin cores was first attributed to reductions in continental ice volume during stadials [*Shackleton et al.*, 2000]. Subsequently, however, a significant contribution from local hydrographic reorganizations has also been identified [*Skinner et al.*, 2003, 2007]. Benthic δ^{18}O values typically decreased gradually by ~0.2–0.5‰ during strong Greenland stadials (e.g., Heinrich stadials) and then increased with the onset of the D-O warm phases (Figure 2). Thus, the benthic oxygen isotope record leads the planktonic δ^{18}O signal by a few hundred years [*Shackleton et al.*, 2000; *Skinner et al.*, 2003, 2007; *Margari et al.*, 2010].

Under modern conditions, Site U1385 is bathed by recirculated North East Atlantic Deep Water, which consists of a mixture of Labrador Sea Water and Iceland-Scotland Overflow Water [*van Aken*, 2000; *Voelker et al.*, 2015; *Jenkins et al.*, 2015]. It is underlain by Lower Deep Water (LDW), a water mass derived from modified Antarctic Bottom Water (AABW). North East Atlantic Deep Water and its glacial counterpart, Glacial North Atlantic Intermediate Water, have different oxygen and carbon isotope signatures than the denser LDW or AABW, despite the attenuation of the Antarctic signature along the flow path. The lower δ^{13}C of AABW and LDW is related to a different source signature and the remineralization of δ^{13}C-depleted organic matter during northward transport. During the last glacial period, the contribution of southern sourced water to the Iberian margin increased relative to northern sources [*Adkins*, 2013]. On millennial time scales, the δ^{13}C values of epibenthic foraminifera are commonly interpreted to reflect variations in North Atlantic Deep Water formation and the Atlantic meridional overturning circulation (AMOC) [*Shackleton et al.*, 2000; *Skinner et al.*, 2007; *Margari et al.*, 2010]. Decreases in benthic δ^{13}C values (reduced AMOC) were abrupt and approximately

Table 1. Age-Depth Tie Points for the Precession-Tuned Age Model

Depth (crmcd)	Precession-Tuned Age (ka)	Sedimentation Rate (cm/ka)
134.58	1184.25	-
140.54	1241.00	10.5
142.03	1260.75	7.5
144.64	1281.00	12.9
146.00	1298.25	7.9
148.48	1314.60	15.2
154.85	1355.70	15.5

synchronous with increases in planktonic δ^{18}O (i.e., Greenland cooling) suggesting a tight coupling of the North Atlantic circulation and climate during the last glacial (Figure 2).

2. Methods

2.1. IODP Site U1385

IODP Expedition 339 ("Mediterranean Outflow") drilled four holes at Site U1385, the "Shackleton Site," on the SW Iberian margin off the Portuguese coast (37°34.285'N, 10°7.562'W, water depth = 2578 m) (Figure 1) [*Hodell et al.*, 2013a]. Site U1385 is located on a structural high, the "Promonotorio dos Principes de Avis," where sedimentation has not been disturbed by turbidity currents [*Hodell et al.*, 2013a]. The recovered sediments were analyzed using core scanning XRF at 1 cm resolution, and the four holes were correlated on the basis of Ca/Ti to form a continuous 165 m long composite section [*Hodell et al.*, 2015]. Here we studied sections 1 to 6 in Core 339-U1385D-15H (123.59–135.82 meter below sea floor (mbsf)) and sections 5 and 6 in Core 339-U1385E-16H (135.24–136.97 mbsf). The splice tie point between the cores occurs at 147.32 corrected revised meters composite depth (crmcd) where U1385D-15H-6, 80 cm is tied to U1385E-16H-5, 59 cm, yielding a ~8 m long section (140.26–148.88 crmcd) spanning MIS 37–41.

2.2. U1385 Chronostratigraphy

Hodell et al. [2015] produced various age models for Site U1385 derived by oxygen isotope stratigraphy, correlation to other records, and orbital tuning. Here we use a revised version of the "insolation-tuned" age model of *Hodell et al.* [2015] developed by correlating sediment lightness L* at Site U1385 to precession (rather than 37°N summer insolation). L* changed in phase with local insolation and lagged precession minima by roughly 3 ka based on L* measurements in the radiometrically dated Core MD99-2334K located nearby [*Skinner et al.*, 2014; *Hodell et al.*, 2015]. We identified one additional age-depth tie point in MIS 40 as sediment color and precession (but not local summer insolation) show a distinct peak around 1300 ka (Figure S1 in the supporting information). No explicit tuning to other orbital parameters was performed, but a fixed response time to local summer insolation was assumed. *Hodell et al.* [2015] justified the validity of the tuning procedure through the amplitude modulation of precession in the depth domain and demonstrated the age model's agreement with the Mediterranean sapropel cyclostratigraphy [*Konijnendijk et al.*, 2014]. Because precession and local summer insolation constitute virtually identical tuning targets (except for the additional tie point), the "precession-tuned" age model is a mere refinement of the "insolation-tuned" age model and is thus supported by the same arguments. Age-depth tie points and sedimentation rates for the study interval are shown in Table 1 and in supporting information Figure S1. Assuming mean sedimentation rates between 7.5 and 15.5 cm/ka, an average temporal resolution of approximately 65 to 130 years was achieved by sampling every centimeter. This is equivalent to or better than most records of millennial-scale climate change during the late Pleistocene and avoids aliasing of the climate signal.

2.3. Stable Isotope Measurements

Twenty specimens of the planktonic foraminifer *Globigerina bulloides* and up to five specimens of the epibenthic species *Cibicidoides wuellerstorfi* were selected for stable isotope analysis at 1 cm intervals from the 250–355 μm and >212 μm size fractions, respectively, to match the methodology of previous studies from MIS 3 [e.g., *Shackleton et al.*, 2000; *Vautravers and Shackleton*, 2006]. Although seasonal productivity and vertical migration of *G. bulloides* might lead to underestimating the absolute amplitude of millennial-scale temperature variability, this applies equally to the previous studies of MIS 3 and hence does not alter our conclusions. Where no *C. wuellerstorfi* specimens were available, *Cibicidoides mundulus* (= *Cibicidoides kullenbergi*) was analyzed instead. In contrast to the epibenthic foraminifer *C. wuellerstorfi*, *C. mundulus* may also exist as a shallow infaunal species. Because of the lowering of pore water C values by organic matter oxidation below the sediment-water interface, δ^{13}C values of *C. mundulus* were disregarded, but δ^{18}O could be used without a correction factor [e.g., *Hodell et al.*, 2008; *Lourens et al.*, 2010; *Hoogakker et al.*, 2010].

Stable isotope measurements of foramini feral calcite were performed at the Godwin Laboratory for Palaeoclimatic Research, Department of Earth Sciences, University of Cambridge. Specimens of *G. bulloides*

were cleaned with a solution of 3% hydrogen peroxide to remove organic contaminants, followed by 10 min ultrasonication in acetone. Benthic specimens were not treated before stable isotope analysis. The tests were crushed, dried overnight at 50°C, and then analyzed on a VG SIRA mass spectrometer with an attached Micromass MultiCarb autosampler or, if samples were smaller than 80 μg, on a Thermo Fisher MAT253 mass spectrometer with a Thermo Fisher Kiel device. The foraminiferal calcite was reacted with 100% orthophosphoric acid in evacuated vials at 70°C, and the resulting CO_2 was analyzed after cryogenic removal of water. A total of 1692 samples was measured in dual inlet mode relative to an in-house reference gas. The gas is calibrated to the Vienna Pee Dee Belemnite standard using international standards. Instrument precision of repeated standard measurements was ±0.06‰ (1σ) for δ^{13}C and ±0.08‰ (1σ) for δ^{18}O.

2.4. Mg/Ca Analysis

Trace metal analysis was performed at the Godwin Laboratory for Palaeoclimatic Research, Department of Earth Sciences, University of Cambridge. Up to 20 specimens of the benthic infaunal foraminifer *Uvigerina peregrina* were selected from samples at ~5–10 cm intervals near the glacial terminations 37/38 and 39/40, using the size fraction >212 μm. The shells were oxidatively cleaned following the scheme by *Barker et al.* [2003] to avoid contamination by clays, organic matter, silicate materials, or other surface coatings. If more than ~240 μg of crushed shell material was available, one third was separated for stable isotopes analysis. Samples were analyzed on a Varian VISTA inductively coupled plasma atomic emission spectroscopy instrument following the intensity ratio calibration method of *de Villiers* [2002]. Instrument precision was better than 0.5% for Mg/Ca from repeated measurements of laboratory standards. The error increased to ~4%–6% for replicates of foraminifera from the same depth. Fe/Ca and Mn/Ca were used to evaluate possible contaminations and show insignificant correlation with Mg/Ca. Deep water temperatures and seawater oxygen isotopic compositions ($\delta^{18}O_w$) were obtained following the methodology of *Elderfield et al.* [2012]. The benthic foraminifer species *U. peregrina* was chosen for the reconstruction because it is less susceptible to the carbonate ion effect than epibenthic species [*Elderfield et al.*, 2012]. The infaunal habitat of *Uvigerina* was presumably constantly saturated for $CaCO_3$ preventing the preferential dissolution of Mg-rich calcite, as proposed initially for the deep infaunal foraminifer *Globobulimina affinis* [*Skinner et al.*, 2003, 2007]. If the number of *U. peregrina* specimens was insufficient for both Mg/Ca and oxygen isotope analyses (23% of all Mg/Ca samples), *U. peregrina* Mg/Ca data were combined with *C. wuellerstorfi* δ^{18}O measurements and used in the $\delta^{18}O_w$ calculations instead. An error propagation for Mg/Ca temperatures and $\delta^{18}O_w$ is provided in the supporting information.

3. Results

3.1. The Glacial-Interglacial Cycles of MIS 37–41

3.1.1. The Benthic δ^{18}O Record

In Figure 3, we present the oxygen and carbon isotopic records of orbital- and millennial-scale climate variability at IODP Site U1385 on the Iberian margin as well as the reconstructed temperature and oxygen isotopic composition of deep water at the study location. Benthic δ^{18}O values averaged ~2.8‰ during MIS 41 and increased gradually into MIS 40. Until the beginning of a gradual deglacial decrease in benthic δ^{18}O at ~1283 ka, benthic δ^{18}O varied between 3.2‰ and 3.9‰ during MIS 40. At ~1288 ka, benthic δ^{18}O decreased rapidly from 3.6‰ to 3.1‰, indicating the beginning of interglacial MIS 39. Benthic δ^{18}O values averaged ~4.1‰ during the peak glacial of MIS 38 (1260 to 1252 ka), which is >0.2‰ higher than peak values during MIS 40. The deglaciation of MIS 38 occurred in two phases. It began with a gradual benthic δ^{18}O decrease at 1254 ka and, in a second stage, accelerated after 1248 ka yielding a 0.7‰ larger total benthic δ^{18}O range than observed during the deglacial process of MIS 40 (~1.5‰ versus ~0.8‰). The substantially different amplitude of the deglacial change is in equal parts the result of stronger glacial conditions (i.e., higher benthic δ^{18}O) during MIS 38 and lower mean benthic δ^{18}O values during MIS 37 (2.7‰) than during the weaker interglacial MIS 39 (3.0‰).

3.1.2. The Deep Water Temperature and the Ice Volume Record

A similar amplitude dichotomy is observed in $\delta^{18}O_w$ but not in deep water temperatures (Figure 3). Mg/Ca paleothermometry of the infaunal benthic foraminifer *U. peregrina* reveals that deep water temperatures were ~0.2°C during both MIS 38 and MIS 40. Interglacial deep water temperatures during MIS 37, MIS 39, and MIS 41 were approximately 3.5°C. $\delta^{18}O_w$ reveals considerable differences between the two glacial cycles, but the reconstruction was limited by an analytical uncertainty of ±0.23‰ SMOW (1σ, see supporting information). During MIS 39–41, $\delta^{18}O_w$ varied approximately between 0.7‰ and 0.3‰, and the transition from MIS 40 to MIS 39 was almost indistinguishable. In contrast, $\delta^{18}O_w$ values briefly reached 1.2‰ in MIS 38

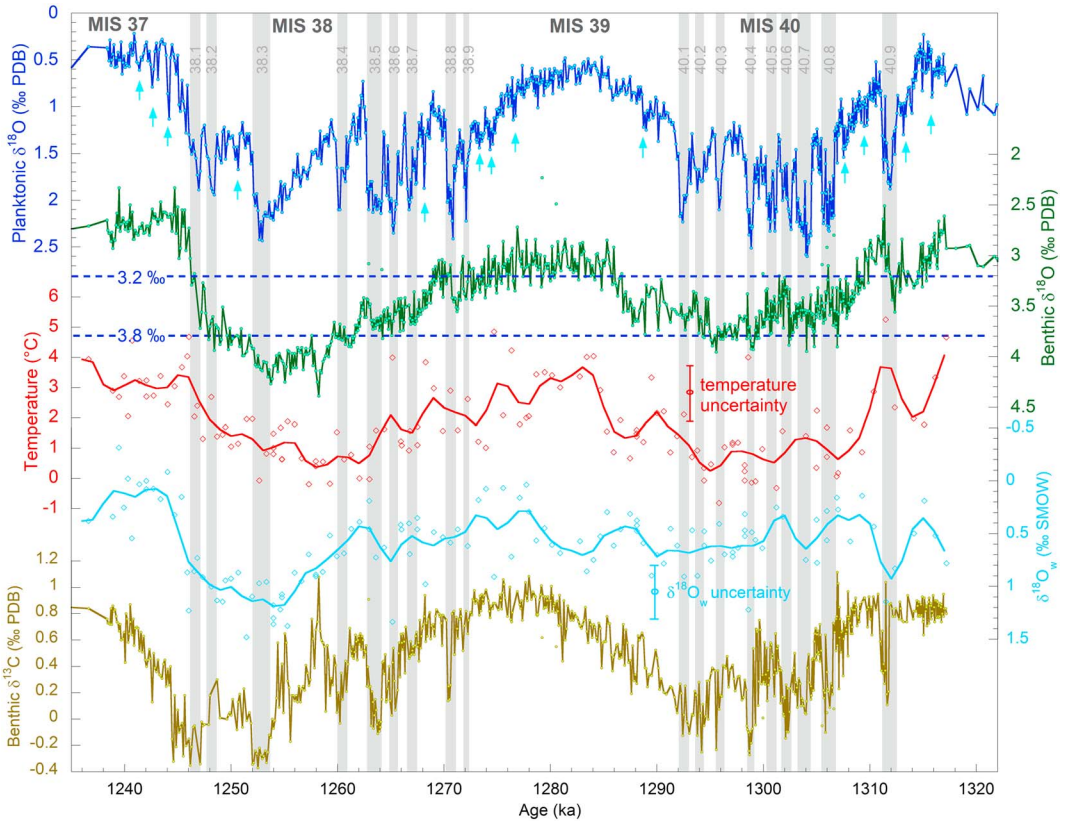

Figure 3. Planktonic $\delta^{18}O$, benthic $\delta^{18}O$, and benthic $\delta^{13}C$ records of millennial-scale variability at Site U1385 on the Iberian margin from marine isotope stages 37 to 41. Mg/Ca temperatures of the infaunal foraminifer *Uvigerina peregrina* are calculated using the core top calibration of *Elderfield et al.* [2010, 2012] and were used to calculate deep water $\delta^{18}O_w$. The red and light blue curves are smoothed signals (5 ka Gaussian filter) of deep water temperature and $\delta^{18}O_w$. The error given for both is the propagated standard error $\pm 1\sigma$. The dashed blue lines drawn at 3.2‰ and 3.8‰ represent the oxygen isotope thresholds of climate instability. Gray bars highlight strong millennial-scale cold events, and arrows indicate events of smaller amplitude.

and decreased abruptly to 0.1‰ during the deglaciation. We did not convert $\delta^{18}O_w$ values to sea level because the oxygen isotope compositions of early Pleistocene ice sheets are highly uncertain and because $\delta^{18}O_w$ on the Iberian margin can also be affected by local hydrographic effects related to deep water circulation [*Skinner et al.*, 2003, 2007].

3.2. Millennial-Scale Variability in MIS 37–41

3.2.1. Suborbital Variability in Planktonic $\delta^{18}O$

Glacials MIS 38 and MIS 40 were characterized by pervasive millennial-scale variability in the planktonic $\delta^{18}O$ record, but millennial variability was suppressed during interglacials MIS 37, MIS 39, and MIS 41 (Figure 3). Cold stadial events during both glacials have been numbered to facilitate the description of the results. Stadials are numbered sequentially from the youngest to the oldest, such that Sx.1 represents the terminal stadial event that occurred just prior to the deglaciation during MIS x. Some weaker cold events are indicated by blue arrows in Figure 3. The inception of glacial MIS 40 was marked by the first strong millennial event (S40.9) at 1312 ka after benthic $\delta^{18}O$ exceeded the threshold of 3.2‰ (blue dashed line in Figure 3). During MIS 40, eight further stadial events (S40.1 to S40.8) were recorded in planktonic $\delta^{18}O$ which had a mean stadial-interstadial range of 1.0±0.16‰. The last stadial event in MIS 40 occurred 6 ka before benthic $\delta^{18}O$ reached interglacial levels in MIS 39 and was followed by a gradual decrease of planktonic $\delta^{18}O$. During MIS 38, a total of nine millennial events (S38.1–S38.9) with an average amplitude of 1.0±0.16‰ was recorded after benthic $\delta^{18}O$ values again exceeded 3.2‰. In contrast to the smaller deglaciation after MIS 40, the termination of MIS 38 occurred in two large, abrupt steps marked by stadial events S38.3 and S38.1. Planktonic $\delta^{18}O$ typically decreased very rapidly from stadial to interstadial levels at the end of each cold event but increased more slowly at their onset giving rise to a sawtooth-like pattern.

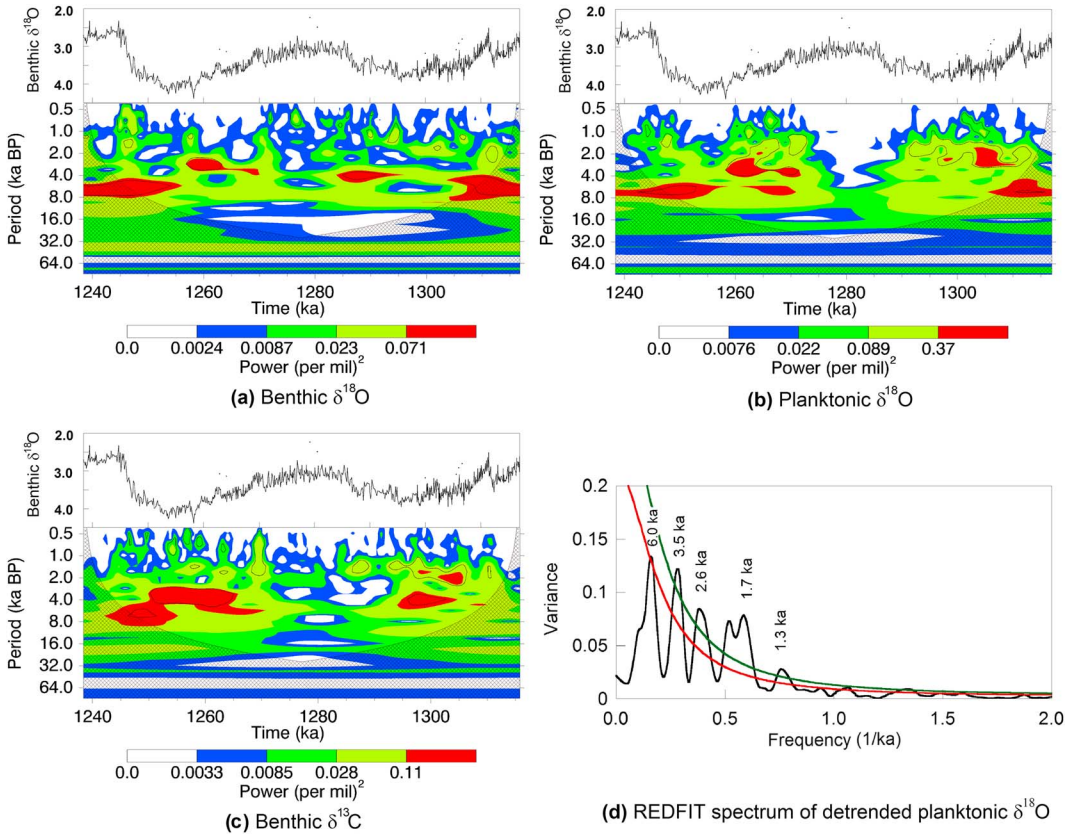

Figure 4. Wavelet analyses of the Site U1385 detrended isotope records including (a) benthic δ^{18}O, (b) planktonic δ^{18}O, and (c) benthic δ^{13}C. Data were detrended by subtracting a 10 ka Gaussian filter from the presmoothed original data (see supporting information). Wavelet plots (Figures 4a–4c) were created using the data analysis tool at http://ion.exelisvis.com/ [*Torrence and Compo*, 1998]. Contour lines give the 95% confidence interval against a red noise background. The hashed area marks the cone of influence where the analysis is affected by edge effects. (d) REDFIT power spectrum [*Schulz and Mudelsee*, 2002] of planktonic δ^{18}O spanning marine isotope stages 37 to 41 (1238.4 to 1317.0 ka). The red and green lines mark the 95% and 80% confidence intervals assuming a red noise model.

3.2.2. Suborbital Variability in Benthic δ^{18}O and δ^{13}C

Considerable millennial-scale variability is also evident in the benthic oxygen and carbon isotope records of Site U1385 (Figure 3). Strong systematic decreases in benthic δ^{18}O and benthic δ^{13}C were associated with most major stadials (i.e., stadials terminated by an abrupt planktonic δ^{18}O decrease of ≥1.0‰) during MIS 38 and 40 (i.e., S38.1, S38.3, S38.4, S38.5, S38.8, S40.4, and S40.6–S40.9 but not S40.1). Benthic δ^{18}O typically decreased quickly by 0.2–0.4‰ at either the start or shortly after each of these stadials developed their full strength in planktonic δ^{18}O and began to return to stadial conditions when planktonic δ^{18}O decreased abruptly. In contrast, benthic δ^{13}C generally decreased almost simultaneously with the increase of planktonic δ^{18}O during the onset of most strong stadials. Coupled changes in planktonic and benthic proxies were evident during termination 37/38 but were lacking during termination 39/40. Some further benthic δ^{13}C variability occurred at 1255 ka and 1258 ka during MIS 38, when benthic δ^{13}C values briefly rose to interglacial levels.

3.2.3. The Pacing of Millennial-Scale Variability

Figure 4 shows the spectral properties of the detrended isotope time series (the detrending procedure is detailed in the supporting information). The REDFIT spectrum [*Schulz and Mudelsee*, 2002] of planktonic δ^{18}O for MIS 37–41 (Figure 4d) reveals that variance is focused primarily at five periods: 1.3 ka, 1.7 ka, 2.6 ka, 3.5 ka, and 6.0 ka. The 1.3 ka, 1.7 ka, 2.6 ka, and 3.5 ka periodicities are significant at the 95% confidence level, whereas the spectral peak at 6.0 ka is only significant at the 80% confidence level against a red noise background. Correspondingly, Morlet wavelet analysis of MIS 37–41 (Figures 4a–4c) detects the highest variance in all three isotope proxies at roughly ~1.5 ka and ~3.5 ka. However, strong variance in the millennial band is exclusive to glacial periods and damped during interglacials. Variance at ~6.5 ka is most prominent during

the deglaciation after MIS 38 as well as the glacial inceptions of MIS 38 and 40. The time series analysis results remain fundamentally unchanged when the "insolation-tuned" age model of *Hodell et al.* [2015] is used instead (see supporting information).

4. Discussion

4.1. Orbital-Scale Variability in MIS 37–41

Previous sea level reconstructions indicate that sea level varied between +20 m and −70 m relative to the Holocene during the glacial-interglacial cycles of MIS 37–41 [*Rohling et al.*, 2014; *Elderfield et al.*, 2012]. MIS 38 was, however, associated with ~10–20 m lower sea level than MIS 40 in both referenced sea level reconstructions. The U1385 benthic $\delta^{18}O$ record is consistent with such intermediate ice volumes during MIS 38 and MIS 40 and puts both glacials into the sea level range estimated for MIS 3. Lower benthic $\delta^{18}O$ values and a considerably stronger $\delta^{18}O_w$ excursion during MIS 38 suggest that MIS 38 was a stronger glacial than MIS 40 despite the comparable deep water temperatures during both glacials. The different strengths of the two glacial-interglacial cycles could be related to ~20 W/m^2 lower 65°N peak summer insolation during MIS 38 and ~15 W/m^2 higher insolation forcing during MIS 37 than MIS 41 because of an eccentricity minimum that occurred during MIS 40.

4.2. Comparing Millennial-Scale Variability in the Early Pleistocene and MIS 3

The millennial variability in the U1385 isotope record of MIS 38 and MIS 40 closely resembled the Dansgaard-Oeschger cycles of MIS 3 in shape, magnitude, and frequency (Figures 3 and 5). Prominent millennial events in MIS 38 and 40 were characterized by a sawtooth-like pattern in planktonic $\delta^{18}O$, similar to the typical shape of D-O events in MIS 3. The mean stadial-interstadial range of 1.0±0.16‰ during both MIS 38 and 40 was virtually identical to the average range of 1.0±0.12‰ recorded during MIS 3 [*Vautravers and Shackleton*, 2006]. Similar suborbital variability during the early Pleistocene and MIS 3 is also evident in the chemical composition of sediments at the Iberian margin [*Hodell et al.*, 2015] as detailed in the supporting information. The pacing of millennial events recognized at Site U1385 compares favorably to the frequencies published for other early Pleistocene records [*Mc Intyre et al.*, 2001; *Raymo et al.*, 1998; *Bailey et al.*, 2012]. *Raymo et al.* [1998] estimated a recurrence interval of 1–5 ka for millennial events, similar to the 2–5 ka range inferred by *Mc Intyre et al.* [2001]. Both estimates are within the range of periods recognized in the time series analysis of the U1385 record (Figure 4). Although the frequency of sub-Milankovitch climate variability in the Pleistocene has been a matter of much debate, the pacing of events at U1385 is also in good agreement with records from the late Pleistocene that indicated primary recurrence intervals between 1 and 2 ka and multiples thereof [*Bond et al.*, 1993; *Schulz*, 2002; *Vautravers and Shackleton*, 2006; *Bond et al.*, 1997; *Dansgaard et al.*, 1993; *Oppo et al.*, 1998].

Weirauch et al. [2008] previously suggested an intensification of millennial variability across the Middle Pleistocene Transition and attributed this change to an increase in mean ice volume from the early to the late Pleistocene. Other studies, in contrast, found evidence of persistent millennial-scale variability that was recorded at comparable magnitude in proxy records prior to the MPT in the eastern North Atlantic [*Raymo et al.*, 1998; *Grützner and Higgins*, 2010; *Hodell et al.*, 2008]. On the basis of the isotope data from Site U1385, we find no significant increase in the magnitude or frequency of millennial events between MIS 37–41 and MIS 3.

Tzedakis et al. [2015] suggested that the succession of stadials and interstadials including S38.5 to S38.7 appeared similar to a late Pleistocene Bond cycle of MIS 3 but without the extreme values associated with Heinrich events. Figure 5 compares the Bond-like cycle from MIS 38 to one example from the last glacial between Heinrich events 5 and 4. A sequence of three stadials that continuously increased in intensity occurred between 1263 and 1270 ka. The sequence culminated in one exceptionally long cold event, highlighted in dark gray. The Bond-like cycle is also reflected by strong variance at ~7 ka in the planktonic $\delta^{18}O$ and benthic $\delta^{13}C$ wavelet plots during that time interval (Figures 4b and 4c). However, identifying further Bond-like cycles in MIS 38 and 40 is ambiguous. Although the lack of additional cycles might be due to the short duration of glacials in the 41 ka world, the occurrence of Bond-like cycles in the early Pleistocene would not necessarily be expected owing to their intrinsic relationship to Heinrich events [*Bond et al.*, 1993] that have not been observed in the early Pleistocene [*Hodell et al.*, 2008].

Despite the similarities of millennial variability in the early and late Pleistocene, *Hodell et al.* [2008] found no evidence of Heinrich events in the geochemical or physical properties of bulk sediments older than 640 ka at IODP Site U1308. Massive ice rafting events from the Hudson Strait are indicated in the U1308 record only after

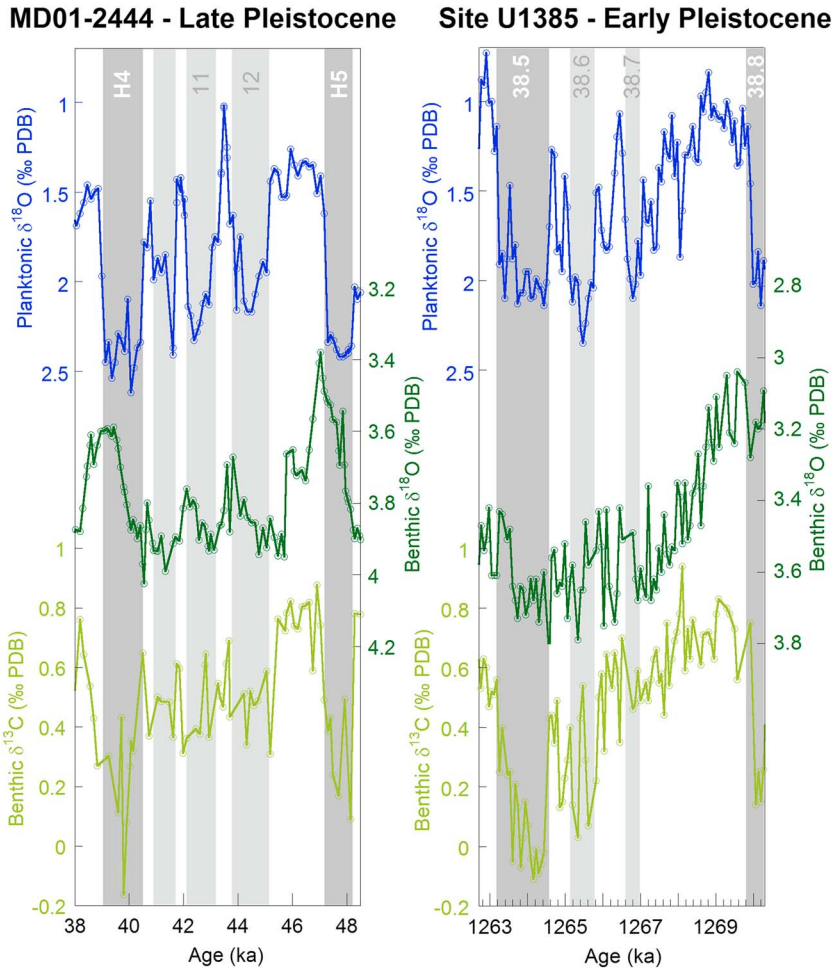

Figure 5. Benthic and planktonic $\delta^{18}O$ as well as benthic $\delta^{13}C$ records from the Iberian margin of a potential Bond-like cycle during marine isotope stage (right) (MIS) 38 compared to an example from (left) MIS 3. Light gray bars highlight normal stadials; dark gray shadings indicate the terminal cold events of each Bond-like cycle (Heinrich events in the case of MIS 3). Late Pleistocene data from *Vautravers and Shackleton* [2006], *Skinner et al.* [2007], *Skinner and Elderfield* [2007], and Skinner (unpublished) are plotted on the SFP04 age scale of *Shackleton et al.* [2004].

prolonged (~50 ka) periods of ice growth, which could not be accomplished during the shorter glacials of the 41 ka world [*Hodell et al.*, 2008]. This implies that the dynamics of the Laurentide ice sheet prior to the MPT may have precluded Heinrich-like events but did not affect the processes responsible for Dansgaard-Oeschger-like events, as presumably all circum-North Atlantic ice sheets contributed to ice rafting in the early Pleistocene [*Bailey et al.*, 2012].

4.3. Climate Thresholds of Millennial-Scale Variability

McManus et al. [1999] proposed that millennial variability was related to an ice volume threshold, such that when ice sheets exceeded a critical size (i.e., when benthic $\delta^{18}O > 3.5‰$), the amplitude and frequency of variability in ice rafting and sea surface temperature proxies increased. However, the physical significance of the 3.5‰ threshold remains uncertain because benthic $\delta^{18}O$ represents a combined signal of temperature and ice volume. Millennial variability was most prominent in the last glacial cycle during MIS 3 when ice volumes reached intermediate levels (~40–90 m sea level equivalent) [*Rohling et al.*, 2014; *Elderfield et al.*, 2012]. As peak ice volumes during the early Pleistocene were mostly confined to this "millennial window" [*Sima et al.*, 2004], the pervasive occurrence of millennial events during the early Pleistocene is perhaps not unexpected. Lower benthic $\delta^{18}O$ thresholds have been suggested for the early Pleistocene, consistent with equally expansive but thinner ice sheets than those of the late Pleistocene [*Raymo et al.*, 1998; *Mc Intyre et al.*, 2001; *Bailey et al.*, 2012]. For example, increased climate variability has been recognized during MIS 40 and MIS 44 when

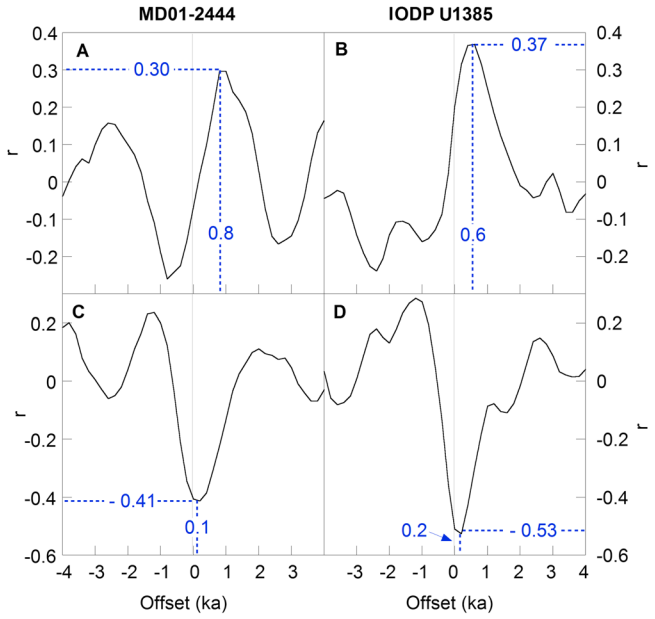

Figure 6. Cross correlation coefficient (*r*) of benthic δ^{18}O and planktonic δ^{18}O from (a) Piston core MD01-2444 (isotope data from *Vautravers and Shackleton* [2006] and *Skinner et al.* [2007] mapped on the Greenland synthetic time scale of *Barker et al.* [2011] by *Hodell et al.* [2013b]) spanning 10 to 60 ka and from (b) Site U1385 spanning marine isotope stages 37 to 41. (c and d) The cross correlation coefficient of planktonic δ^{18}O and benthic δ^{13}C for the same locations and periods instead. Positive offsets denote a lead of benthic δ^{18}O over planktonic δ^{18}O in Figures 6a and 6b or a lead of planktonic δ^{18}O over benthic δ^{13}C in Figures 6d and 6d, respectively. The smoothed time series were detrended by subtracting a 10 ka trend from the interpolated original data (see supporting information). The isolated high-frequency component was analyzed using the cross correlation function of Analyseries [*Paillard et al.*, 1996].

benthic δ^{18}O values were between 3.3‰ and 3.8‰ [*Raymo et al.*, 1998]. Similarly, *Mc Intyre et al.* [2001] suggested the onset of pronounced millennial climate variability when benthic δ^{18}O exceeded 3.3‰ to 3.5‰ during the period from 1.75 to 1.83 Ma.

In Figure 3, the benthic δ^{18}O threshold for the onset of strong millennial variability at the Iberian margin is estimated to be 3.2‰ which was crossed during both glacial inceptions. Millennial-scale variability was suppressed during the interglacials MIS 37, MIS 39, and MIS 41. An upper threshold may occur at 3.8‰, as suggested by the lack of millennial events between stadials S38.4 and S38.3 but is less certain. Some further planktonic δ^{18}O excursions were recorded in MIS 37–41 outside the defined thresholds, but their amplitude and frequency were considerably reduced (blue arrows in Figure 3).

Threshold behavior appears to be an intrinsic feature of millennial variability throughout the Pleistocene, suggesting that the same processes could be responsible for confining the window of climate instability. Presumably, millennial variability was activated when ice sheets became large enough to reach the coast and interact with the ocean, but thresholds could also indicate low temperatures that permitted abrupt climate change—for example, by sea ice advance in the Nordic Seas [*Li et al.*, 2005, 2010; *McManus et al.*, 1999].

4.4. The Bipolar See-Saw and Freshwater Forcing in the 41 ka World

Methane synchronization of ice core records from Greenland and Antarctica revealed asynchronous temperature changes between the two hemispheres on millennial time scales during the last glacial [e.g., *Blunier and Brook*, 2001; *Blunier et al.*, 1997; *Steig and Alley*, 2002; *Blunier et al.*, 1998]. This bipolar see-saw pattern has been explained by variability of the meridional overturning circulation [*Broecker*, 1998; *Stocker and Johnsen*, 2003]. When deep water formation in the North Atlantic was weakened, less heat was advected by the surface currents from the tropics to high Northern latitudes and the Iberian margin cooled. At the same time, Antarctica warmed because of the reduced heat transport from south to north across the equator. A sudden resumption of the overturning circulation reversed the trends and quickly warmed the North Atlantic region.

At the Iberian margin, these changes were coregistered by different proxies and were reflected in the relative phasing of planktonic and benthic δ^{18}O variability [*Shackleton et al.*, 2000; *Skinner et al.*, 2003; *Shackleton et al.*, 2004]. *Shackleton et al.* [2000] observed that benthic δ^{18}O led planktonic δ^{18}O on millennial time scales. Although the reasons for local benthic δ^{18}O variability are complex, this lead has been interpreted to reflect the asymmetry of temperature variability between the Northern and Southern Hemispheres [*Margari et al.*, 2010, 2014; *Martrat et al.*, 2007]. Parallel changes in benthic δ^{13}C were found to be broadly antiphased to planktonic δ^{18}O, suggesting an association between the surface cooling, interhemispheric heat transport, and perturbations of the meridional overturning circulation during the late Pleistocene [*Martrat et al.*, 2007; *Shackleton et al.*, 2000; *Skinner et al.*, 2007].

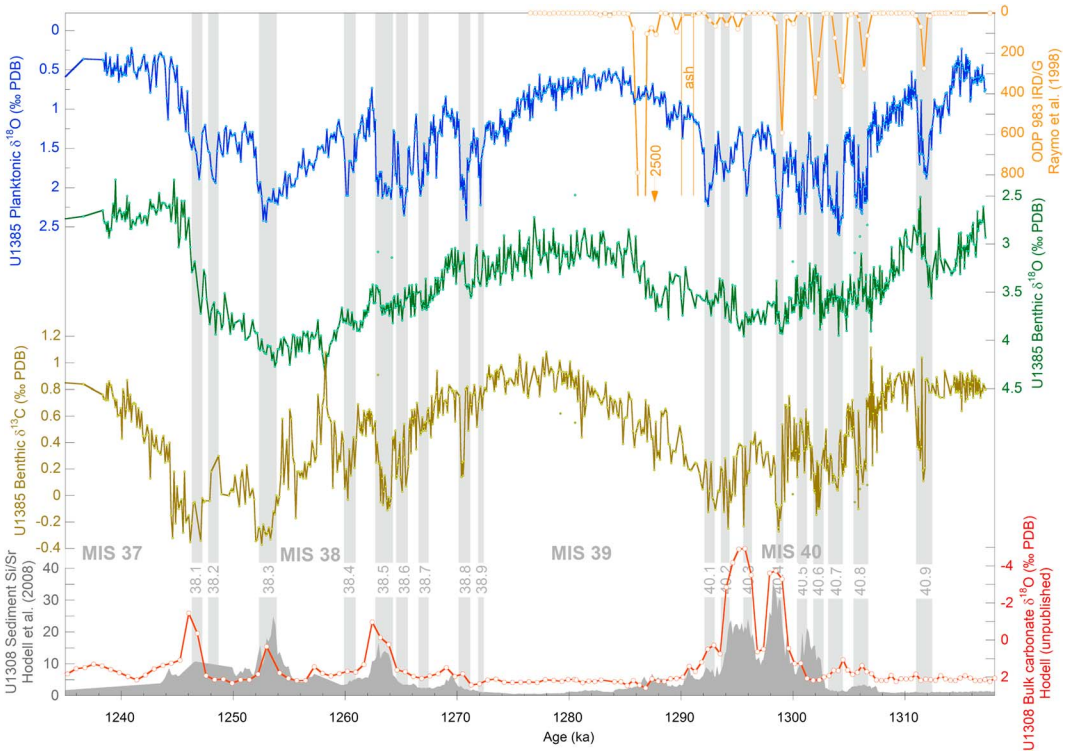

Figure 7. Comparison of the U1385 Iberian margin isotope record with different ice rafting proxies. The records of Sites ODP 983 [*Raymo et al.*, 1998], IODP U1308 [*Hodell et al.*, 2008], and IODP U1385 have been aligned by correlating their benthic δ^{18}O curves (see supporting information) and are all shown on the "precession-tuned" age scale of this study. An ash layer is highlighted in the ODP Site 983 record [*Raymo et al.*, 1998]. Sediment Si/Sr and bulk carbonate δ^{18}O at IODP Site U1308 have been shown to correlate with IRD input at the site in the late Pleistocene [*Hodell et al.*, 2008].

The relative phasing of the Site U1385 isotope records suggests an active oceanic bipolar see-saw in the 41 ka world of the early Pleistocene. The most prominent stadials in MIS 38 and 40 (i.e., stadials terminated by an abrupt planktonic δ^{18}O decrease of $\geq$1.0‰ except for S40.1) were associated with simultaneous AMOC anomalies, as indicated by benthic δ^{13}C (Figures 3 and 5). However, mean benthic δ^{13}C values were slightly lower during the early Pleistocene than MIS 3, perhaps reflecting a generally weakened overturning circulation during the interval or changes in the biological pump in the source regions of North Atlantic Deep Water and AABW. As in the last glacial, the decline of planktonic δ^{18}O at the end of major stadials was preceded by a decrease in benthic δ^{18}O. Benthic δ^{18}O decreases, however, were slightly smaller but more abrupt than during the last glacial, similar to observations from MIS 6 [*Margari et al.*, 2010]. Some (less prominent) stadials were not associated with noticeable decreases in benthic δ^{18}O and δ^{13}C at Site U1385. It remains unclear whether potential AMOC perturbations were too small to become apparent in the Iberian margin proxy records or whether the decoupling of the isotope records reflects the true lack of a thermal bipolar see-saw during these events.

Cross correlation of the detrended planktonic and benthic isotope records was performed to quantify their relative phasing and is presented in Figure 6 (for detailed methods see supporting information). The cross correlation function of Analyseries [*Paillard et al.*, 1996] was used to calculate correlation coefficients and identify the leads and lags between the detrended time series. Figure 6 shows that the cross correlation of the MIS 37–41 isotope time series resembles the results of MIS 3. This method estimates a ~0.6 ka lead of benthic δ^{18}O over planktonic δ^{18}O in the early Pleistocene. Planktonic δ^{18}O in turn was approximately antiphased to benthic δ^{13}C. A cross correlation analysis of the early Pleistocene record in the depth domain yields similar lag times (see supporting information). Thus, the phase relationships between the proxy records support the operation of an oceanic bipolar see-saw, analogous to that observed in the last glacial period, (at least) during major millennial events in the early Pleistocene.

The similarity in shape, pacing, amplitude, and relative phasing of millennial-scale variability in surface and deep climate records from MIS 38 and MIS 40 in the early Pleistocene and MIS 3 suggests a common mechanism for millennial variability across the MPT despite the large changes in long-term mean climate state. Once a certain climate threshold (coinciding with intermediate ice volumes) was crossed, D-O and possibly Bond-like cycles were initiated during early Pleistocene glacials. In addition, the pattern of millennial variability is suggestive of an active bipolar see-saw during strong stadials. Although this parallels observations from the late Pleistocene, the absence of Heinrich events during MIS 38 and 40 [*Hodell et al.*, 2008] reveals substantial differences in the dynamics of the Laurentide ice sheet, suggesting that different processes were responsible for Heinrich event-like climate perturbations.

Freshwater-induced changes in the strength of the thermohaline circulation are one of the leading hypotheses to explain abrupt climate change [e.g., *Broecker*, 1994; *Shackleton et al.*, 2000], but the role of freshwater in triggering stadial events has recently been challenged [*Barker et al.*, 2015]. Freshwater from circum-North Atlantic ice sheets may have disrupted the oceanic density structure and reduced or prevented deep water formation. Consistent with proxy evidence, the climate impacts of AMOC perturbations would be most strongly felt in Greenland and the North Atlantic [e.g., *Liu et al.*, 2009; *Vellinga and Wood*, 2002; *Manabe and Stouffer*, 1997; *Menviel et al.*, 2014; *Kageyama et al.*, 2010; *Manabe and Stouffer*, 1988; *Ganopolski and Rahmstorf*, 2001].

Figure 7 shows that millennial-scale variability on the Iberian margin can be linked to evidence of ice rafting at other locations in the North Atlantic. Most of the six IRD peaks at Ocean Drilling Program (ODP) Site 983 [*Raymo et al.*, 1998] are closely aligned with six major increases in planktonic δ^{18}O at the Iberian margin during MIS 40. The IRD proxies, Si/Sr, and bulk carbonate δ^{18}O from IODP Site U1308 [*Hodell et al.*, 2008] also support a connection of stadial events to ice rafting. However, not all IRD events found at Site 983 are detected at Site U1308. This probably reflects that IRD from different source regions is captured in the two records. Nevertheless, the correlation of the three records strongly suggests a relationship between ice surging (IRD, Si/Sr, and bulk carbonate δ^{18}O peaks), perturbations of the meridional overturning circulation (lower benthic δ^{13}C), and surface cooling (higher planktonic δ^{18}O) consistent with freshwater forcing of the thermohaline circulation during MIS 38 and 40. A similar relationship between ice rafting and overturning circulation has been suggested previously [*Raymo et al.*, 1998; *Hodell et al.*, 2008]. However, it remains uncertain whether the association of ice rafting and stadials in the early Pleistocene reflects iceberg melting that triggered AMOC anomalies or instead indicates that iceberg melting merely enhanced AMOC perturbations and North Atlantic cooling during already established stadials [*Barker et al.*, 2015].

5. Conclusion

Millennial-scale variability in surface temperature (inferred from planktonic δ^{18}O) on the Iberian margin was very strong during glacials MIS 38 and MIS 40, demonstrating that it was a persistent feature of the early Pleistocene glacial periods when glacial-interglacial cycles were occurring regularly at a period of 41 ka. Millennial-scale variability in the late Pleistocene is best expressed during intermediate ice volume states (~40–90 m sea level equivalent) when benthic δ^{18}O values were between 3.5‰ and ~4.5‰ [*McManus et al.*, 1999]. Considering that the climate system spent a great amount of time in this "millennial window" [*Sima et al.*, 2004] during the early Pleistocene, it is perhaps not unexpected that millennial variability was such a prominent feature of glacial climate in the 41 ka world [*Raymo et al.*, 1998; *Mc Intyre et al.*, 2001; *Bailey et al.*, 2012].

Millennial variability was suppressed during interglacial periods (MIS 37, MIS 39, and MIS 41) and was activated during glacial inceptions when benthic δ^{18}O exceeded 3.2‰. A comparison of planktonic δ^{18}O values during glacials MIS 38 and 40 to observations of the last glacial period (MIS 3) reveals a high similarity of millennial-scale climate variability in terms of amplitude, shape, and pacing. Benthic and planktonic δ^{18}O show an asymmetric relative phasing consistent with the operation of an oceanic thermal bipolar see-saw during most strong stadials in the early Pleistocene, similar to that observed during the last glacial. Many of the prominent stadials in MIS 38 and 40 were associated with perturbations of the meridional overturning circulation, as indicated by low benthic δ^{13}C values. Furthermore, most stadials on the Iberian margin can be correlated with IRD events at high-latitude sites in the North Atlantic, suggesting a role of freshwater forcing in the generation or amplification of millennial-scale variability.

Our data provide strong evidence of similar millennial-scale climate cycles during the early Pleistocene and MIS 3. Their great similarity implies that millennial variability may have been driven by a common mechanism

before and after the Middle Pleistocene Transition despite the large changes in climatic boundary conditions. However, an unanswered question is whether millennial-scale variability is merely a symptomatic feature of glacial climate or whether it, alternatively, takes an active role in the inception and/or termination of glacial cycles. Improved understanding of the interaction of millennial- and orbital-scale climate variability will lead to a more complete explanation for the observed patterns of climate change during the Pleistocene ice ages.

Acknowledgments
The data presented in this paper are archived on the PANGAEA and NOAA Paleoclimate data systems. This work was made possible by a DAAD scholarship and NERC grant NE/K005804/1. Linda and Jeannie Booth as well as John Nicolson are thanked for laboratory support. We are grateful for James Rolfe's and Ian Mather's expert stable isotope analyses, Simon Crowhurst's assistance with time series analyses, and Mervyn Greaves' insightful comments on Mg/Ca paleothermometry. This manuscript was greatly improved by reviews from Ian Bailey and two anonymous reviewers.

References

Adkins, J. F. (2013), The role of deep ocean circulation in setting glacial climates, *Paleoceanography*, *28*, 539–561, doi:10.1002/palo.20046.
Ashkenazy, Y., and E. Tziperman (2004), Are the 41 kyr glacial oscillations a linear response to Milankovitch forcing?, *Quat. Sci. Rev.*, *23*(18), 1879–1890, doi:10.1016/j.quascirev.2004.04.008.
Bailey, I., G. L. Foster, P. A. Wilson, L. Jovane, C. D. Storey, C. N. Trueman, and J. Becker (2012), Flux and provenance of ice rafted debris in the earliest Pleistocene sub-polar North Atlantic Ocean comparable to the last glacial maximum, *Earth Planet. Sci. Lett.*, *341–344*, 222–233, doi:10.1016/j.epsl.2012.05.034.
Barker, S., M. Greaves, and H. Elderfield (2003), A study of cleaning procedures used for foraminiferal Mg/Ca paleothermometry, *Geochem. Geophys. Geosyst.*, *4*(9), 8407, doi:10.1029/2003GC000559.
Barker, S., G. Knorr, R. Edwards, and F. Parrenin (2011), 800,000 years of abrupt climate variability, *Science*, *334*, 347–352, doi:10.1126/science.1203580.
Barker, S., J. Chen, X. Gong, L. Jonkers, G. Knorr, and D. Thornalley (2015), Icebergs not the trigger for North Atlantic cold events, *Nature*, *520*, 333–336, doi:10.1038/nature14330.
Bazin, L., et al. (2013), An optimized multi-proxy, multi-site Antarctic ice and gas orbital chronology (AICC2012): 120–800 ka, *Clim. Past*, *9*, 1715–1731, doi:10.5194/cp-9-1715-2013.
Blunier, T., and E. J. Brook (2001), Timing of millennial-scale climate change in Antarctica and Greenland during the last glacial period, *Science*, *291*, 109–112, doi:10.1126/science.291.5501.109.
Blunier, T., et al. (1997), Timing of the Antarctic cold reversal and the atmospheric CO_2 increase with respect to the Younger Dryas Event, *Geophys. Res. Lett.*, *24*(21), 2683–2686, doi:10.1029/97GL02658.
Blunier, T., J. Chappellaz, J. Schander, A. Dallenbach, B. Stauffer, T. F. Stocker, D. Raynaud, J. Jouzel, H. B. Clausen, C. U. Hammer, and S. J. Johnsen (1998), Asynchrony of Antarctic and Greenland climate change during the last glacial period, *Nature*, *394*, 739–743, doi:10.1038/29447.
Bond, G. C., and R. Lotti (1995), Iceberg discharges into the North Atlantic on millennial time scales during the last glaciation, *Science*, *267*, 1005–1010, doi:10.1126/science.267.5200.1005.
Bond, G. C., W. S. Broecker, S. Johnsen, J. McManus, L. Babeyrie, J. Jouzel, and G. Bonani (1993), Correlations between climate records from North Atlantic sediments and Greenland ice, *Lett. Nat.*, *365*, 143–147, doi:10.1038/365143a0.
Bond, G. C., W. Showers, M. Cheseby, R. Lotti, P. Almasi, P. DeMenocal, P. Priore, H. Cullen, I. Hajdas, and G. Bonani (1997), A pervasive millennial-scale cycle in North Atlantic Holocene and glacial climates, *Science*, *278*, 1257–1266, doi:10.1126/science.278.5341.1257.
Broecker, W. S. (1994), Massive iceberg discharges as triggers for global climate change, *Nature*, *372*, 421–424, doi:10.1038/372421a0.
Broecker, W. S. (1998), Paleocean circulation during the Last Deglaciation: A bipolar seesaw?, *Paleoceanography*, *13*(2), 119–121, doi:10.1029/97PA03707.
Clark, P. U., D. Archer, D. Pollard, J. D. Blum, J. A. Rial, V. Brovkin, A. C. Mix, N. G. Pisias, and M. Roy (2006), The middle Pleistocene transition: Characteristics, mechanisms, and implications for long-term changes in atmospheric pCO_2, *Quat. Sci. Rev.*, *25*(23–24), 3150–3184, doi:10.1016/j.quascirev.2006.07.008.
Dansgaard, W., et al. (1993), Evidence for general instability of past climate from a 250-kyr ice-core record, *Nature*, *364*, 218–210, doi:10.1038/364218a0.
Denton, G. H., R. F. Anderson, J. R. Toggweiler, R. L. Edwards, J. M. Schaefer, and A. E. Putnam (2010), The last glacial termination, *Science*, *328*, 1652–1656, doi:10.1126/science.1184119.
de Villiers, S. (2002), An intensity ratio calibration method for the accurate determination of Mg/Ca and Sr/Ca of marine carbonates by ICP-AES, *Geochem. Geophys. Geosyst.*, *3*, 1001, doi:10.1029/2001GC000169.
Elderfield, H., M. Greaves, S. Barker, I. R. Hall, A. Tripati, P. Ferretti, S. J. Crowhurst, L. Booth, and C. Daunt (2010), A record of bottom water temperature and seawater $\delta^{18}O$ for the Southern Ocean over the past 440 kyr based on Mg/Ca of benthic foraminiferal Uvigerina spp, *Quat. Sci. Rev.*, *29*(1–2), 160–169, doi:10.1016/j.quascirev.2009.07.013.
Elderfield, H., P. Ferretti, S. J. Crowhurst, I. N. Mccave, D. A. Hodell, and A. M. Piotrowski (2012), Evolution of ocean temperature and ice volume through the mid-Pleistocene climate transition, *Science*, *337*, 704–710, doi:10.1126/science.1221294.
European Project for Ice Coring in Antarctica Community Members (2006), One-to-one coupling of glacial climate variability in Greenland and Antarctica, *Nature*, *444*, 195–198, doi:10.1038/nature05301.
Ganopolski, A., and S. Rahmstorf (2001), Rapid changes of glacial climate simulated in a coupled climate model, *Nature*, *409*, 153–158, doi:10.1038/35051500.
Grützner, J., and S. M. Higgins (2010), Threshold behavior of millennial scale variability in deep water hydrography inferred from a 1.1 Ma long record of sediment provenance at the southern Gardar Drift, *Paleoceanography*, *25*, PA4204, doi:10.1029/2009PA001873.
Hodell, D. A., J. E. T. Channell, J. H. Curtis, O. E. Romero, and U. Röhl (2008), Onset of "Hudson Strait" Heinrich events in the eastern North Atlantic at the end of the middle Pleistocene transition (~640 ka)?, *Paleoceanography*, *23*, PA4218, doi:10.1029/2008PA001591.
Hodell, D. A., L. Lourens, D. V. Stow, J. Hernández-Molina, C. Alvarez Zarikian, and the Shackleton Site Project Members (2013a), The "Shackleton Site" (IODP Site U1385) on the Iberian margin, *Sci. Drilling*, *16*, 13–19, doi:10.5194/sd-16-13-2013.
Hodell, D. A., S. J. Crowhurst, L. Skinner, P. C. Tzedakis, V. Margari, J. E. T. Channell, G. Kamenov, S. Maclachlan, and G. Rothwell (2013b), Response of Iberian Margin sediments to orbital and suborbital forcing over the past 420 ka, *Paleoceanography*, *28*, 185–199, doi:10.1002/palo.20017.
Hodell, D. A., L. Lourens, S. J. Crowhurst, T. Konijnendijk, R. Tjallingii, F. Jimenez-Espejo, L. C. Skinner, P. C. Tzedakis, and Members of the Shackleton Site Project (2015), A reference time scale for Site U1385 (Shackleton Site) on the Iberian Margin, *Global Planet. Change*, *133*, 49–64, doi:10.1016/j.gloplacha.2015.07.002.
Hoogakker, B., H. Elderfield, K. Oliver, and S. Crowhurst (2010), Benthic foraminiferal oxygen isotope offsets over the last glacial-interglacial cycle, *Paleoceanography*, *25*, PA4229, doi:10.1029/2009PA001870.
Imbrie, J., et al. (1992), On the structure and origin of major glaciation cycles 1. Linear responses to Milankovitch forcing, *Paleoceanography*, *7*(6), 701–738, doi:10.1029/92PA02253.

Imbrie, J., et al. (1993), On the structure and origin of major glacation cycles 2. The 100,000-year cycle, *Paleoceanography*, *8*(6), 699–735, doi:10.1029/93PA02751.
Jenkins, W. J., W. M. Smethie Jr., E. A. Boyle, and G. A. Cutter (2015), Water mass analysis for the U.S. GEOTRACES (GA03) North Atlantic Sections, *Deep Sea Res., Part II*, *116*, 6–20, doi:10.1016/j.dsr2.2014.11.018.
Johnsen, S. J., H. B. Clausen, W. Dansgaard, K. Fuhrer, N. Gundestrup, C. U. Hammer, P. Iversen, J. Jouzel, B. Stauffer, and J. P. Steffensen (1992), Irregular glacial interstadials recorded in a new Greenland ice core, *Nature*, *359*, 311–313, doi:10.1038/359311a0.
Jouzel, J., et al. (2007), Orbital and millennial Antarctic climate variability over the past 800,000 years, *Science*, *317*, 793–796, doi:10.1126/science.1141038.
Kageyama, M., A. Paul, D. M. Roche, and C. J. Van Meerbeeck (2010), Modelling glacial climatic millennial-scale variability related to changes in the Atlantic meridional overturning circulation: A review, *Quat. Sci. Rev.*, *29*(21), 2931–2956, doi:10.1016/j.quascirev.2010.05.029.
Konijnendijk, T. Y. M., M. Ziegler, and L. J. Lourens (2014), Chronological constraints on Pleistocene sapropel depositions from high-resolution geochemical records of ODP Sites 967 and 968, *Newslett. Stratigraphy*, *47*(3), 263–282, doi:10.1127/0078-0421/2014/0047.
Li, C., D. S. Battisti, D. P. Schrag, and E. Tziperman (2005), Abrupt climate shifts in Greenland due to displacements of the sea ice edge, *Geophys. Res. Lett.*, *32*, L19702, doi:10.1029/2005GL023492.
Li, C., D. S. Battisti, and C. M. Bitz (2010), Can North Atlantic sea ice anomalies account for Dansgaard-Oeschger climate signals?, *J. Clim.*, *23*, 5457–5475, doi:10.1175/2010JCLI3409.1.
Lisiecki, L. E., and M. E. Raymo (2005), A Pliocene-Pleistocene stack of 57 globally distributed benthic δ^{18}O records, *Paleoceanography*, *20*, PA1003, doi:10.1029/2004PA001071.
Liu, Z., et al. (2009), Transient simulation of last deglaciation with a new mechanism for Bolling-Allerod warming, *Science*, *325*, 310–314, doi:10.1126/science.1171041.
Lourens, L. J., J. Becker, R. Bintanja, F. J. Hilgen, E. Tuenter, R. S. W. van de Wal, and M. Ziegler (2010), Linear and non-linear response of late Neogene glacial cycles to obliquity forcing and implications for the Milankovitch theory, *Quat. Sci. Rev.*, *29*(1–2), 352–365, doi:10.1016/j.quascirev.2009.10.018.
Manabe, S., and R. J. Stouffer (1988), Two stable equilibria of a coupled ocean-atmosphere model, *J. Clim.*, *1*, 841–866, doi:10.1175/1520-0442(1988)001<0841:TSEOAC>2.0.CO;2.
Manabe, S., and R. J. Stouffer (1997), Coupled ocean-atmosphere model response to freshwater input: Comparison to Younger Dryas event, *Paleoceanography*, *12*(2), 321–336, doi:10.1029/97PA01763.
Margari, V., L. C. Skinner, P. C. Tzedakis, A. Ganopolski, M. J. Vautravers, and N. J. Shackleton (2010), The nature of millennial-scale climate variability during the past two glacial periods, *Nat. Geosci.*, *1*, G35070, doi:10.1038/ngeo740.
Margari, V., L. C. Skinner, D. A. Hodell, B. Martrat, S. Toucanne, J. O. Grimalt, P. L. Gibbard, J. P. Lunkka, and P. C. Tzedakis (2014), Land-ocean changes on orbital and millennial time scales and the penultimate glaciation, *Geology*, *42*(3), 183–186, doi:10.1130/G35070.1.
Martrat, B., J. O. Grimalt, N. J. Shackleton, L. de Abreu, M. A. Hutterli, and T. F. Stocker (2007), Four climate cycles of recurring deep and surface water destabilizations on the Iberian margin, *Science*, *317*, 502–507, doi:10.1126/science.1139994.
Maslin, M. a., and C. M. Brierley (2015), The role of orbital forcing in the early middle Pleistocene transition, *Quat. Int.*, *389*, 47–55, doi:10.1016/j.quaint.2015.01.047.
Mc Intyre, K., M. L. Delaney, and A. C. Ravelo (2001), Millennial-scale climate change and oceanic processes in the Late Pliocene and Early Pleistocene, *Paleoceanography*, *16*(5), 535–543, doi:10.1029/2000PA000526.
McManus, J. F., D. W. Oppo, and J. L. Cullen (1999), A 0.5-million-year record of millennial-scale climate variability in the North Atlantic, *Science*, *283*, 971–975, doi:10.1126/science.283.5404.971.
Menviel, L., A. Timmermann, T. Friedrich, and M. H. England (2014), Hindcasting the continuum of Dansgaard-Oeschger variability: Mechanisms, patterns and timing, *Clim. Past*, *10*, 63–77, doi:10.5194/cp-10-63-2014.
North Greenland Ice Core Project Members (2004), High-resolution record of Northern Hemisphere climate extending into the last interglacial period, *Nature*, *431*, 147–151, doi:10.1038/nature02805.
Oeschger, H., J. Beer, U. Siegenthaler, B. Stauffer, W. Dansgaard, and C. Langway (1984), Late glacial climate history from ice cores, in *Climate Processes and Climate Sensitivity*, edited by J. E. Hansen and T. Takahashi, pp. 299–306, AGU, Washington, D. C., doi:10.1029/GM029p0299.
Oppo, D. W., J. F. McManus, and J. L. Cullen (1998), Abrupt climate events 500,000 to 340,000 years ago: Evidence from subpolar North Atlantic sediments, *Science*, *279*, 1335–1338, doi:10.1126/science.279.5355.1335.
Paillard, D., L. Labeyrie, and P. Yiou (1996), Macintosh program performs time-series analysis, *Eos Trans. AGU*, *77*(39), 379, doi:10.1029/96EO00259.
Raymo, M., K. Ganley, S. Carter, D. Oppo, and J. McManus (1998), Millennial-scale climate instability during the early Pleistocene epoch, *Nature*, *542*, 699–702, doi:10.1038/33658.
Raymo, M. E., and K. Nisancioglu (2003), The 41 kyr world: Milankovitch's other unsolved mystery, *Paleoceanography*, *18*, 1011, doi:10.1029/2002PA000791.
Rohling, E. J., G. L. Foster, K. M. Grant, G. Marino, A. P. Roberts, M. E. Tamisiea, and F. Williams (2014), Sea-level and deep-sea-temperature variability over the past 5.3 million years, *Nature*, *508*, 477–482, doi:10.1038/nature13230.
Ryan, W. B. F., et al. (2009), Global multi-resolution topography synthesis, *Geochem. Geophys. Geosyst.*, *10*, Q03014, doi:10.1029/2008GC002332.
Schulz, M. (2002), On the 1470-year pacing of Dansgaard-Oeschger warm events, *Paleoceanography*, *17*(2), 1014, doi:10.1029/2000PA000571.
Schulz, M., and M. Mudelsee (2002), REDFIT: Estimating red-noise spectra directly from unevenly spaced paleoclimatic time series, *Comput. Geosci.*, *28*, 421–426, doi:10.1016/S0098-3004(01)00044-9.
Shackleton, N. J., M. A. Hall, and E. Vincent (2000), Phase relationships between millennial-scale events 64,000–24,000 years, *Paleoceanography*, *15*(6), 565–569, doi:10.1029/2000PA000513.
Shackleton, N. J., R. G. Fairbanks, T. Chiu, and F. Parrenin (2004), Absolute calibration of the Greenland time scale: Implications for Antarctic time scales and for Δ14C, *Quat. Sci. Rev.*, *23*(14–15), 1513–1522, doi:10.1016/j.quascirev.2004.03.006.
Sima, A., A. Paul, and M. Schulz (2004), The younger Dryas—An intrinsic feature of late Pleistocene climate change at millennial timescales, *Earth Planet. Sci. Lett.*, *222*, 741–750, doi:10.1016/j.epsl.2004.03.026.
Skinner, L. C., and H. Elderfield (2007), Rapid fluctuations in the deep North Atlantic heat budget during the last glacial period, *Paleoceanography*, *22*, PA1205, doi:10.1029/2006PA001338.

Skinner, L. C., N. J. Shackleton, and H. Elderfield (2003), Millennial-scale variability of deep-water temperature and $\delta^{18}O_{dw}$ indicating deep-water source variations in the Northeast Atlantic, 0–34 cal. ka BP, *Geochem. Geophys. Geosyst.*, *4*(12), 1098, doi:10.1029/2003GC000585.

Skinner, L. C., H. Elderfield, and M. A. Hall (2007), Phasing of millennial climate events and Northeast Atlantic deep-water temperature change since 50 ka BP, in *Ocean Circulation: Mechanisms and Impacts—Past and Future Changes of Meridional Overturning, Geophys. Monogr. Ser.*, vol. 173, edited by A. Schmittner, J. C. H. Chiang, and S. R. Hemming, pp. 197–208, AGU, Washington, D. C., doi:10.1029/173GM14.

Skinner, L. C., C. Waelbroeck, A. E. Scrivner, and S. J. Fallon (2014), Radiocarbon evidence for alternating northern and southern sources of ventilation of the deep Atlantic carbon pool during the last deglaciation., *Proc. Natl. Acad. Sci. U.S.A.*, *111*(15), 5480–5484, doi:10.1073/pnas.1400668111.

Steig, E. J., and R. B. Alley (2002), Phase relationships between Antarctica and Greenland climate records, *Ann. Glaciol.*, *35*, 451–456, doi:10.3189/172756402781817211.

Stocker, T. F., and S. J. Johnsen (2003), A minimum thermodynamic model for the bipolar seesaw, *Paleoceanography*, *18*(4), 1087, doi:10.1029/2003PA000920.

Torrence, C., and G. P. Compo (1998), A practical guide to wavelet analysis, *Bull. Am. Meteorol. Soc.*, *79*(1), 61–78, doi:10.1175/1520-0477(1998)079<0061:APGTWA>2.0.CO;2.

Tzedakis, P. C., V. Margari, and D. Hodell (2015), Coupled ocean-land millennial-scale changes 1.26 million years ago, recorded at Site U1385 off Portugal, *Global Planet. Change*, *135*, 83–88.

van Aken, H. M. (2000), The hydrography of the mid-latitude Northeast Atlantic Ocean II: The intermediate water masses, *Deep Sea Res., Part II*, *47*, 789–824, doi:10.1016/S0967-0637(99)00112-0.

Vautravers, M. J., and N. J. Shackleton (2006), Centennial-scale surface hydrology off Portugal during marine isotope stage 3: Insights from planktonic foraminiferal fauna variability, *Paleoceanography*, *21*, PA3004, doi:10.1029/2005PA001144.

Vellinga, M., and R. A. Wood (2002), Global climatic impacts of a collapse of the Atlantic thermohaline circulation, *Clim. Change*, *54*, 251–267, doi:10.1023/A:1016168827653.

Voelker, A. H. L., and L. de Abreu (2011), A review of abrupt climate change events in the Northeastern Atlantic Ocean (Iberian margin): Latitudinal, longitudinal and vertical gradients., in *Abrupt Climate Change: Mechanisms, Patterns, and Impacts, Geophys. Monogr. Ser.*, vol. 193, edited by H. Rashid, L. Polyak, and E. Mosley-Thompson, pp. 15–37, AGU, Washington, D. C., doi:10.1029/2010GM001021.

Voelker, A. H. L., A. Colman, G. Olack, J. J. Waniek, and D. Hodell (2015), Oxygen and hydrogen isotope signatures of Northeast Atlantic water masses, *Deep Sea Res., Part II*, *116*, 89–106, doi:10.1016/j.dsr2.2014.11.006.

Weirauch, D., K. Billups, and P. Martin (2008), Evolution of millennial-scale climate variability during the mid-Pleistocene, *Paleoceanography*, *23*, PA3216, doi:10.1029/2007PA001584.